Accepted version of the article:

Reimann, T., Rehrl, C., Shoemaker, W. B., Geyer, T., Birk, S. (2011): The significance of turbulent flow representation in single-continuum models. Water Resources Research 47, W09503, doi:10.1029/2010WR010133.

The significance of turbulent flow representation in single-continuum models

Thomas Reimann[1,*], Christoph Rehrl[2] (†), W. Barclay Shoemaker[3], Tobias Geyer[4], Steffen Birk[2]

1,*) Corresponding author: Thomas Reimann, TU Dresden, Institute for Groundwater Management, D-01062 Dresden, Germany, email: Thomas.Reimann@tu-dresden.de, phone: +49 351 46342555, Fax: +49 351 46342552;

2) University of Graz, Institute for Earth Sciences, Heinrichstrasse 26, A-8010 Graz, Austria, email: steffen.birk@uni-graz.at, phone: +43 316 380 5583;

3) U.S. Geological Survey, 3110 SW 9th Ave, Fort Lauderdale, Florida 33315, USA, email: bshoemak@usgs.gov, phone: +1 954 377 5956;

4) University of Göttingen, Geoscientific Centre, Goldschmidtstrasse 3, D-37077 Göttingen, Germany, email: tgeyer@gwdg.de, phone: +49 551 39 9398

Keywords: karst hydrology; groundwater flow; numerical modeling; dual porosity; turbulent flow

AGU Index Terms: 1828 Groundwater hydraulics

Abstract

Karst aquifers exhibit highly conductive features caused from rock dissolution processes. Flow within these structures can become turbulent and therefore be expressed by nonlinear gradient functions. One way to account for these effects is by coupling a continuum model with a conduit network. Alternatively, turbulent flow can be considered by adapting the hydraulic conductivity within the continuum model. Consequently, the significance of turbulent flow on the dynamic behavior of karst springs is investigated by an enhanced single-continuum model that results in conduit-type flow in continuum cells – CTFc. The single-continuum approach CTFc represents laminar and turbulent flow as well as more complex hybrid models that require additional programming and numerical efforts. A parameter study is conducted to investigate effects of turbulent flow on the response of karst springs to recharge events using the new CTFc approach, existing hybrid models, and MODFLOW-2005. Results reflect the importance of representing (1) turbulent flow in karst conduits and (2) the exchange between conduits and continuum cells. More specifically, laminar models overestimate maximum spring discharge and underestimate hydraulic gradients within the conduit. It follows that aquifer properties inferred from spring hydrographs are potentially impaired by ignoring flow effects due to turbulence. The exchange factor used for hybrid models is necessary to account for the scale dependency between hydraulic properties of the matrix continuum and conduits. This functionality, which is not included in CTFc, can be mimicked by appropriate use of the Horizontal Flow Barrier package for MODFLOW.

1. Introduction

Karst aquifers can be conceptualized as dual-flow systems comprised of (1) fractured porous rock-matrix (defined herein as matrix) with high storage-capacity, which includes primary or intergranular porosity and secondary porosity due to fractures, and (2) highly permeable solution conduits (tertiary porosity) with relatively high-velocity flow and low storage-capacity. These conduits form together with the surrounding matrix a complex and heterogeneous flow system. Commonly, flow in the low permeability matrix is laminar. Conversely, flow in the discrete and localized solution conduits is rapid and therefore often turbulent. Hydraulic signals, such as pulse discharge due to recharge events, are rapidly transmitted through solution conduits both in pressurized and open-channel flow [e.g. Covington et al., 2009]. Karst springs often respond quickly and strongly to recharge events. During recession periods, however, conduit flow is sustained by draining the storage provided by the matrix [Ford and Williams, 2007]. To simulate responses of hydraulic heads and spring discharge to recharge events, the solution conduit and matrix flow processes need to be linked. Numerical models that incorporate this linkage are often used for this purpose. Appropriate modeling approaches frequently employed for this reason are described by Teutsch and Sauter [1998].

In accordance with the dual-flow conceptual model, flow in the matrix can be treated as a continuum flow field, whereas flow in the conduit system is simulated using a discrete pipe network that accounts for both laminar and turbulent flow conditions. Hybrid models (HM) coupling continuum and discrete approaches are frequently employed for generic modeling in basic research, e.g., to simulate and analyze flow and transport processes [for example Király, 1984; Eisenlohr et al., 1997; Birk et al., 2006] or the mechanism of speleogenesis [for example Liedl et al., 2003; Rehrl et al., 2008; Kaufmann, 2009]. Recently, Hill et al. [2010] applied the United States Geological Survey (USGS) hybrid model Conduit

Flow Process Mode 1 (CFPM1) [Shoemaker et al., 2008a] to simulate transient flow in the karst aquifer of Weeki Wachee, in west central Florida. In general, hybrid models are rarely applied to real aquifer systems as they require detailed information on aquifer geometry, hydraulic parameters, and boundary conditions, which often are not available. Further, the computational efforts of such hybrid models are considerable and the practical compatibility with existing model-related tools like graphical user interfaces, calibration tools, or other model packages is fairly limited.

On the contrary, single-continuum models (SCM) are more frequently used for practical applications because they offer several advantages, e.g. lower parameter requirements, reduced numerical demands, and easily accessible codes. Such models represent conduit influenced areas by highly conductive cells (smeared conduit approach; Painter et al. [2006], Worthington [2009]) within an SCM. Commonly, groundwater flow in SCMs such as MODFLOW-2005 [Harbaugh, 2005] is computed using the Darcy equation, which considers laminar flow only and therefore ignores potential effects of turbulence. Scanlon et al. [2003] used an SCM to simulate regional groundwater flow at Barton Springs Edwards aquifer (Texas). The authors conclude that the model cannot, however, accurately simulate local directions or rate of groundwater flow because major conduits are not explicitly designated and turbulent flow is not represented. Lindgren et al. [2004] also simulated the Edwards aquifer (Texas) with a laminar SCM and found similar results, concluding that the incorporation of turbulent flow could facilitate a better simulation of groundwater flow and transport.

One alternative approach to apply SCMs on a local scale is to represent conduits with relatively small model cells that allow laminar and turbulent flow. The Conduit Flow Process Mode 2 (CFPM2) [Shoemaker et al., 2008a] for MODFLOW-2005 [Harbaugh, 2005] is a promising new method that accounts for turbulent flow in the continuum. Originally, this approach was intended to reflect flow conditions in highly permeable, stratiform porous layers ("vuggy layers") [Shoemaker et al., 2008a, b; Kuniansky et al., 2008]. A newly developed modification of CFPM2 considers turbulent flow more generally using a user defined nonlinearity of flow [Reimann et al., 2011]. Setting the parameter that controls the nonlinearity to an appropriate value results in conduit-type flow in continuum cells, subsequently shortened as CTFc.

The objective of this work is to answer the following questions: (1) Is it possible to simulate groundwater flow affected by strong local heterogeneities with a continuum approach that accounts for laminar and turbulent flow? (2) Is this laminar and turbulent continuum model appropriate to reflect the dual-flow behavior of karst aquifers, resulting from matrix-conduit interaction? (3) What is the relevance of turbulent conduit flow with respect to the dynamic responses typically observed at karst springs? To consider these questions, SCM approaches are compared with HM approaches that are known to provide adequate representations of the dual-flow behavior of karst aquifers [Birk et al., 2005; Hill et al., 2010]. The SCM approaches employed include the aforementioned CFPM2, which is intended to represent turbulent flow in vuggy layers, and the modified version of CFPM2 representing CTFc.

To this end, equations to describe turbulent flow in discrete structures are assembled. Subsequently, the flow equation originally intended for the laminar continuum is re-derived to analogously consider turbulent conduit-type flow – CTFc – with appropriate parameters. Next, CTFc is applied to simulate a coupled matrix-conduit system representing a hypothetical karst catchment. In extension to Covington et al. [2009], who examined the transmission of recharge pulses through single elements of karst aquifers, this application considers the signal transmission through a coupled conduit-matrix system. CTFc results are validated by comparison with existing numerical approaches that explicitly consider turbulent conduit flow. Furthermore, the influence of the matrix as well as the conduit-matrix interaction on conduit flow was studied. Finally, the article discusses the differences between the turbulent continuum approach CTFc and existing continuum (MODFLOW-2005) as well as hybrid (CFPM1) models with emphasis on future applications.

2. Description of Karst Aquifer Hydraulics

Governing laminar and turbulent flow equations are presented with the aim of incorporating turbulent flow in continuum cells. The transition between laminar and turbulent flow is governed by the dimensionless Reynolds number [Bear, 1988]:

$$\mathrm{Re} = \frac{q d^*}{\nu} \tag{1}$$

where q denotes the specific discharge [L/T] defined as discharge per unit cross section flow area, d* is some specific length dimension [L] (mean void diameter of porous media or conduit diameter for discrete elements), and ν is the kinematic viscosity of the fluid [L^2/T].

2.1 Flow Processes in the Matrix

Slow and laminar groundwater flow in the matrix along the i-th direction is computed using the linear Darcy equation,

$$q_i = -K_i \frac{\partial h}{\partial x_i} \tag{2}$$

where K is the hydraulic conductivity [L/T], h represents the hydraulic head [L], and x is the spatial coordinate along flow direction [L]. The Darcy equation is valid for laminar flow as long as the Reynolds number does not exceed a value of around 1 to 10 [Bear, 1988].

More generally, flow processes can be described with polynomial laws. A universal formulation is presented by Muskat [1946]

$$\frac{\partial h}{\partial x_i} = \beta_1 q_i + \beta_2 q_i^m \tag{3}$$

where m represents the constant exponential term of the power law, which is assumed to take values between 1 and 2 [*Şen*, 1995], and β_1 [T/L] as well as β_2 [T^m/L^m] are parameters related to fluid and rock properties. The linear term of the polynomial covers laminar flow and can be interpreted as the Darcy equation with hydraulic conductivity $K = 1/\beta_1$. The nonlinear term describes turbulent flow by a power law. Several empirical and semi-empirical power laws can be derived from this equation to account for turbulent flow [*Şen*, 1995]. A common expression was suggested by Forchheimer [1901] with m = 2.0. For turbulent flow conditions (Re >> 10) with high specific discharge the linear term in equation 3 becomes small and therefore can be neglected.

2.2. Flow Processes in Conduits

Subsequently, equations for discrete flow in cylindrical conduits with circular cross-section are described in order to transfer the characteristics to the continuum flow model. Existing HMs like CFPM1 [Shoemaker et al., 2008a] or CAVE [Liedl et al., 2003] consider one-dimensional flow processes in karst conduits using the Darcy-Weisbach approach [Young et al., 2004]

$$\frac{\partial h}{\partial x} = -\mu \frac{q^2}{2gd} \tag{4}$$

where μ represents the friction coefficient [–], which controls the flow regime, d is the conduit diameter, and g denotes the gravitational acceleration [L/T^2]. Laminar flow in cylindrical conduits is described with the linear Hagen-Poiseuille equation that can be obtained from the Darcy-Weisbach approach if μ = 64/Re [Young et al., 2004]

$$q = -\frac{gd^2}{32\nu}\frac{\partial h}{\partial x} \qquad (5)$$

Therefore, laminar flow in the matrix and the conduits (compare equation 2) is described with structurally similar equations resulting in equivalent flow characteristics (Figure 1).

A critical Reynolds number Re_c of about 2,000 [Jain, 2001] characterizes the transition from laminar ($Re < Re_C$) to turbulent flow conditions ($Re > Re_C$) in cylindrical pipes. Furthermore, turbulent flow conditions can be subdivided into a transition zone (slightly turbulent with Reynolds numbers moderately exceeding Re_C) and a fully turbulent zone [Jain, 2001]. Turbulent flow in cylindrical conduits can be represented by the Colebrook-White equation [Young et al., 2004], which is also based on the Darcy-Weisbach approach (equation 4)

$$q = -2\log\left(\frac{k_c}{3.71d} + \frac{2.51\nu}{d\sqrt{2gd\frac{\partial h}{\partial x}}}\right)\sqrt{2gd\frac{\partial h}{\partial x}} \qquad (6)$$

where k_c denotes roughness [L]. The Colebrook-White equation covers flow in the transition zone as well as in the fully turbulent zone. The relation between specific discharge q and hydraulic gradient $(\partial h/\partial x)$ is

$$q \propto \log\left(c + \frac{1}{\sqrt{\frac{\partial h}{\partial x}}}\right)\sqrt{\frac{\partial h}{\partial x}} \qquad (7)$$

with c representing some constant value. The logarithmic term in equation 7 approaches a constant value (log c) with increasing hydraulic gradient resulting in similarity to the nonlinear term of the generalized power law with m = 2.0 (equation 3).

Alternatively, turbulent flow can be described with Manning's equation [Jain, 2001], which is primarily intended for free-surface flow but is also applicable for karst conduits, for example Peterson and Wicks [2006] and Meyer et al., [2008]

$$q = \frac{1}{n}\left(r_{hy}\right)^{\frac{2}{3}}\sqrt{\frac{\partial h}{\partial x}} \qquad (8)$$

where n represents the Manning coefficient [$T/L^{(1/3)}$] and r_{hy} is the hydraulic radius [L] (equal to cross section flow area divided by wetted perimeter). The Manning equation considers turbulent flow in the fully turbulent zone by a power law relation

$$q \propto \sqrt{\frac{\partial h}{\partial x}} \qquad (9)$$

and, therefore, equals the nonlinear term of the generalized power law (equation 3) with an exponential term m = 2.0. Because Manning's equation is widespread in environmental hydraulics, several references regarding parameterization are available (Table 1).

Table 1: Values for Manning coefficient n.

Description	**Value for Manning coefficient n [s/m$^{(1/3)}$]**	**Author**
Natural channel, earth, smooth	0.020	Jain [2001]
Natural channel with gravel beds, straight	0.025	Jain [2001]
Natural channel with gravel beds, with boulders	0.040	Jain [2001]
Karst conduits (Devil's Icebox – Connor's Cave System in central Missouri, model application)	0.035	Peterson and Wicks [2006]

Figure 1 illustrates the relation between specific discharge and hydraulic gradient for an example situation (d = 0.2 m, k_c = 0.01 m, n = 1.83 x 10^{-2} s/$m^{(1/3)}$). For considerably turbulent conditions the Colebrook-White equation equals the Manning equation and also the generalized power law with m = 2.0. Consequently, the Colebrook-White and Manning equation can be converted into each other using the relation [Jain, 2001]

$$n \propto k_c^{\frac{1}{6}} \tag{10}$$

where the adequate conversion can be found by empirical investigations, for instance as n = (1/24) $k_c^{(1/6)}$ [Jain, 2001]. Hence, for hydraulic situations typically found in karst systems the Colebrook-White and the Manning equation produce similar results (compare equations 7, 9, and Figure 1).

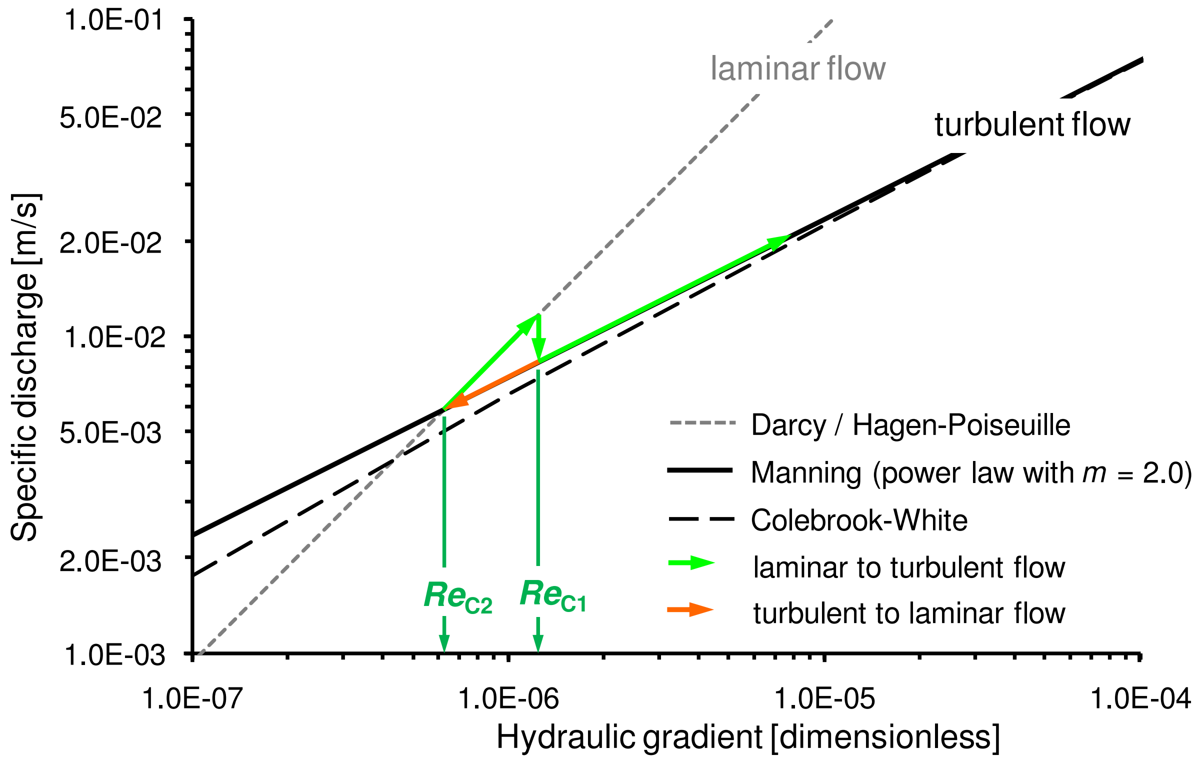

Figure 1: Hydraulic gradient and corresponding discharge for different linear (laminar flow) and nonlinear (turbulent flow) equations. The example is computed for a conduit with d = 0.2 m, k_c = 0.01 m, and n = 1.83 x 10^{-2} s/m$^{(1/3)}$.

While transitioning from laminar to turbulent flow and vice versa, conduit flow may be influenced by hysteresis effects, as laminar flow tends to stay laminar and turbulent flow tends to stay turbulent. This effect is observed for pipes by several authors [Kanda and Yanagiya, 2008]. The hysteresis process is described by two critical Reynolds numbers as shown in Figure 1. Re_{C1} denotes the transition from laminar to turbulent flow conditions and Re_{C2} represents the transition from turbulent to laminar flow conditions. Depending on the values for Re_{C1} and Re_{C2}, discharge may exhibit a step-wise behavior while transitioning between these two regimes. Hence, these two critical Reynolds numbers are considered during laminar and turbulent flow computation.

2.3. Interaction between Matrix and Conduit Flow

Both matrix and conduits interact with each other resulting in the aforementioned dual flow characteristics. The hydraulic parameters of the matrix are influenced by small scale fissures and fractures. The hydraulic conductivity of the matrix at a field-relevant length scale, therefore, is expected to be higher than that at laboratory scale (0 – 1 m) [Kiraly, 2002]. This scale-dependency of hydraulic properties needs to be addressed when investigating the interaction between matrix and karst conduits. Figure 2 shows the cross-section of a conceptual model of a karst conduit draining the matrix and the associated flow components and capacities. The different flow components are described in more detail below. This conceptual interpretation is based on several assumptions as subsequently denoted and aims to give a simplified overview of the importance of the individual components.

240 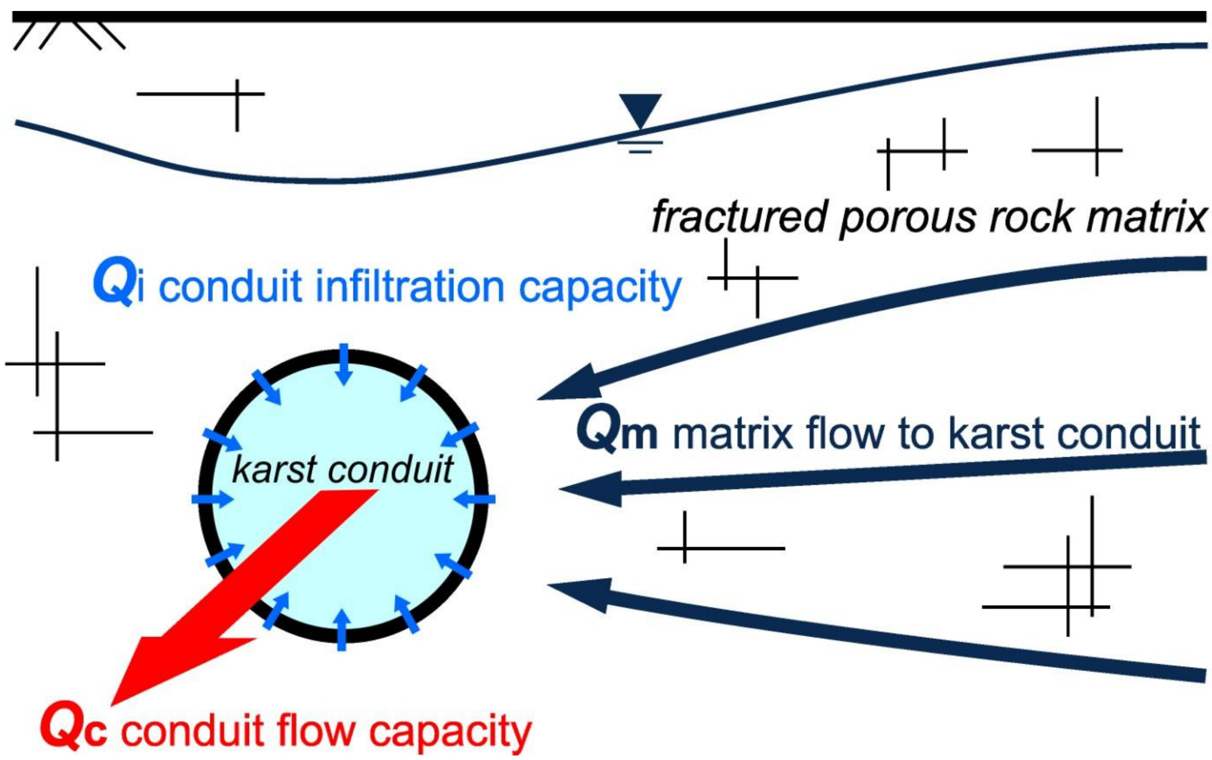

241 **Figure 2:** Cross section of a karst conduit embedded in the matrix. The flow system is
242 controlled by matrix flow to karst conduits (Q_m), conduit infiltration capacity (Q_i), and
243 conduit flow capacity (Q_c).

<u>(Q_m/L) Flow in the matrix toward karst conduits and vice versa</u> is the volumetric flow rate provided by the matrix due to the hydraulic gradient in the matrix induced by the conduit. This flow can be approximated with the equations for steady flow in an unconfined homogeneous aquifer as [Bear, 1988]

$$\frac{Q_m}{L} = K_{m1} \frac{h_0^2 - h_1^2}{\Lambda} \tag{11}$$

where Q_m/L represents matrix flow to or from the karst conduit [L^2/T] per unit length, K_{m1} is the hydraulic conductivity of the matrix for a sufficient length scale [L/T], h_0 is the hydraulic head [L] at the distance Λ [L] perpendicular to the conduit flow direction [L] and h_1 is the hydraulic head [L] in the matrix at the conduit. Note that equation 11 covers the flow to the conduit from both sides.

<u>(Q_i/L) The conduit infiltration capacity</u> is the volumetric flow rate per unit length that can be gathered by the cylindrical karst conduit based on Darcy's equation

$$\frac{Q_i}{L} = \pi d K_{m2} I_{m2} \tag{12}$$

where Q_i/L represents the infiltration capacity of the conduit [L^2/T] per unit length, K_{m2} is the hydraulic conductivity of the matrix in the direct vicinity of the conduit [L/T], and I_{m2} denotes the dimensionless inflow gradient between karst conduit and matrix. The conduit infiltration capacity can be affected by clastic, organic and precipitated sediments deposited in a karst conduit, e.g. wall coatings and crystal growth (details about cave interior deposits can be found in Ford and Williams [2007]). In general, K_{m2} is smaller than K_{m1} due to increased influence of fissures and fractures at larger scale as mentioned above.

<u>(Q_c) Conduit flow capacity</u> is calculated for laminar flow conditions with a linear flow equation (e.g., Hagen-Poiseuille equation) and for turbulent flow conditions with nonlinear flow equations (e.g., Colebrook-White equation, Manning equation). Consequently, the hydraulic gradient inside the conduit I_c depends on discharge, which represents the balance of inflow and outflow per unit length along the conduit flow direction. Accordingly, the conduit flow capacity affects the infiltration capacity Q_i/L.

The flow components Q_m/L , Q_i/L, and Q_c control the event-induced hydraulic signal transmission in terms of discharge and head in both the karst conduit and the matrix. Depending on the amount of water gathered by the conduit, a hydraulic gradient in the matrix (approximated as I_{m1}), which drives water toward the draining conduit, and a hydraulic gradient between conduit and matrix (I_{m2}) can be determined. Consider, for example, a karst aquifer with a single conduit 0.2 m in diameter. The amount of water gathered by the conduit per unit length is assumed to be 3 x 10^{-7} m^2/s (compare Figure 3, arrow 1) inducing a gradient I_{m1} in the matrix, approximated by the head difference (assuming the matrix head near the conduit is related to the conduit perimeter $h_1 = \pi d/2$) perpendicular to the conduit divided by the associated length, which was set equal to 100 m. This gradient depends on the matrix hydraulic conductivity for a sufficient length scale K_{m1}, which is assumed to be 1 x 10^{-5} m/s (compare Figure 3, arrow 2a). The inflow gradient I_{m2} was calculated for the hydraulic conductivity in the vicinity of the conduit K_{m2}, which is assumed to be 1 x 10^{-9} m/s (compare Figure 3, arrow 2b). Since the inflow gradient I_{m2} of 4 x 10^2 is significantly increased compared to the matrix gradient of 1 x 10^{-2}, it is expected that for this specific parameter set under the assumed conditions, matrix heads significantly exceed the conduit heads in order to obtain the necessary hydraulic gradient between the conduit and the matrix.

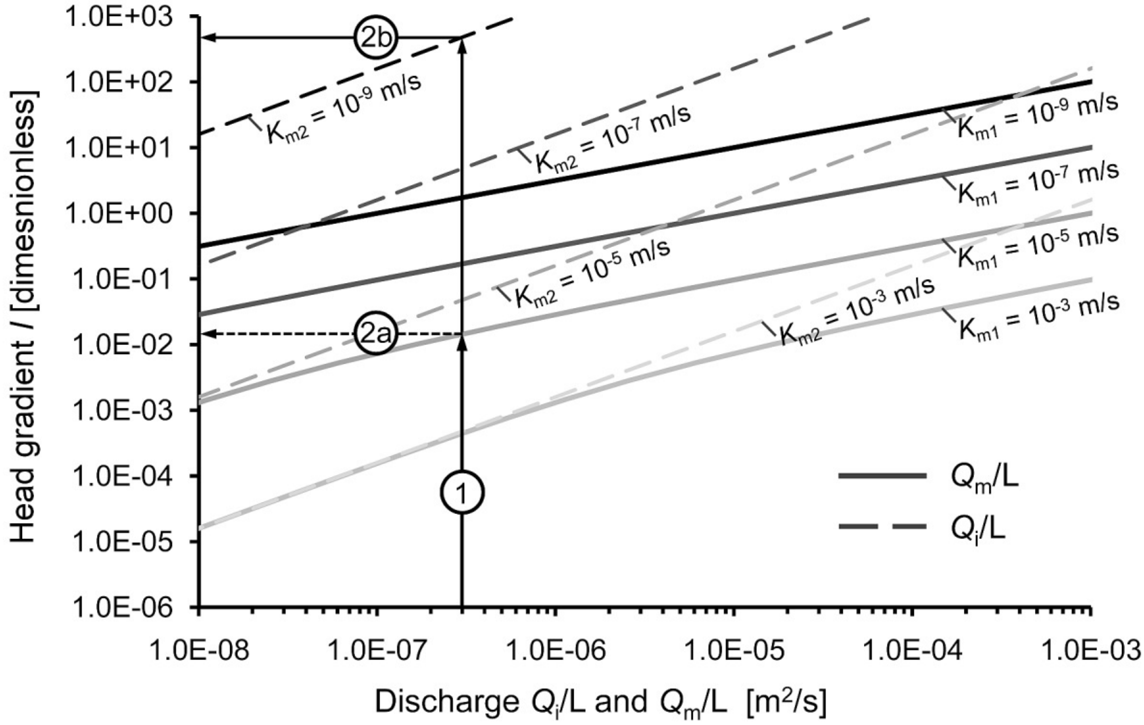

Figure 3: Flow rates Q_m/L and Q_i/L for a karst system with a single conduit (d = 0.2 m) for several hydraulic conductivities. With a given amount of water that is gathered by the conduit (Step 1), one can determine the equivalent hydraulic gradient in the matrix towards the conduit. In this example the gradient is approximated by the head difference (assuming $h_o = \pi d/2$) perpendicular to the conduit divided by the associated length, which was set equal to 100 m (Step 2a: $K_{m1} = 1 \times 10^{-5}$ m/s). The necessary inflow gradient I_{m2} for the conduit can be determined according to the hydraulic conductivity in the matrix in the vicinity of the conduit K_{m2} (Step 2b: $K_{m2} = 1 \times 10^{-9}$ m/s). As the inflow gradient I_{m2} clearly exceeds the matrix gradient, matrix heads will clearly exceed conduit heads for this specific parameter set under the assumed conditions.

3. Numerical Computation of Turbulent Flow in Karst Aquifers

3.1. Hybrid Models

To account for the three conduit-flow components (Figure 3), a hybrid model may be applied, which couples the discrete conduit network and the continuous matrix flow field by a head-dependent linear transfer term [Barenblatt et al., 1960; Bauer et al., 2003]

$$Q_{ex} = \alpha A_{ex} K_{m2} \left(h_m - h_c\right) = f_{ex} L K_{m1} \left(h_m - h_c\right) \tag{13}$$

where Q_{ex} represents the exchange flow rate [L^3/T], α [1/L] is a factor that depends on the conduit geometry and may be interpreted as inverse distance related to the head difference, A_{ex} [L^2] is the exchange area between conduit and matrix, h_m is the hydraulic head in the matrix [L], and h_c represents the hydraulic head in the conduit [L]. Water exchange may also be described as a function of the matrix hydraulic conductivity K_{m1}, which is used for the continuum model, and the conduit length L [L] by use of a dimensionless exchange factor f_{ex}. Accordingly, the exchange factor allows controlling the conduit infiltration capacity Q_i/L. This could be necessary as the matrix hydraulic conductivity used for the continuum may be higher than that in the vicinity of the conduit. The reason for this behavior is the scale dependency of hydraulic properties [Kiraly, 2002], compare section 2.3. Consequently, the necessary gradient to capture Q_m/L (flow towards the conduit) by Q_i/L (conduit infiltration capacity) is large. This scaling issue can be addressed by an adequately chosen value of f_{ex}. If f_{ex} exceeds a certain threshold value, no additional flow resistance between conduit and matrix exists and flow is limited by the matrix only. Bauer et al. [2003] observed this behavior while investigating the influence of the exchange factor on karst aquifer genesis. Further information regarding the numerical computation of laminar and turbulent flow in discrete structures coupled to a continuum can be found in the literature [e.g. Liedl et al., 2003; Shoemaker et al., 2008a].

3.2. Turbulent Single-Continuum Models

Standard groundwater continuum models ignore turbulent flow conditions and, therefore, potentially represent pipe flow by a Darcian approach. An exception is CFPM2 for MODFLOW-2005 [Shoemaker et al., 2008a], which considers turbulent flow effects within continuum cells based on an approach introduced by Halford [2000]. MODFLOW-2005 [Harbaugh 2005] computes three-dimensional laminar groundwater flow in the matrix with the following equation

$$\frac{\partial}{\partial x}\left(K_{xx}\frac{\partial h_m}{\partial x}\right)+\frac{\partial}{\partial y}\left(K_{yy}\frac{\partial h_m}{\partial y}\right)+\frac{\partial}{\partial z}\left(K_{zz}\frac{\partial h_m}{\partial z}\right)\pm\psi=S_s\left(\frac{\partial h_m}{\partial t}\right) \tag{14}$$

where K_{xx}, K_{yy}, and K_{zz} are the hydraulic conductivities [L/T] along the x, y, and z axes respectively, ψ is the external volumetric flux per unit volume and represents sources and/or sinks of water [1/T], S_s is the specific storage [1/L], and t is time [T]. In the case of turbulent flow conditions, CFPM2 modifies the horizontal hydraulic conductivity as a nonlinear function in terms of head gradient and critical head gradient. Initially, CFPM2 was intended to account for turbulent flow in aquifers with large pores where the turbulence occurs at low Reynolds number (1 to 100) [Kuniansky et al., 2008; Shoemaker et al., 2008a, b]. Reimann et al. [2011] modified CFPM2 to consider turbulent flow with a user defined flow exponent m (compare equation 3) such that the code is potentially able to account for conduit-type flow in continuum cells – CTFc. Subsequently, the differences between the existing and modified CFPM2 approaches are briefly introduced.

Karst conduits are represented in CFPM2 by continuum cells, which are indicated by a very high hydraulic conductivity and adequately small spatial discretization. To obtain values for the hydraulic conductivity, the Hagen-Poiseuille equation (equation 5) can be combined with the Darcy equation (equation 2) yielding the conduit hydraulic conductivity for laminar conditions $K_{lam,c}$ [L/T]

$$K_{lam,c} = \frac{gd^2}{32\nu} \tag{15}$$

As stated in the previous section 2.2., the transition from laminar to turbulent flow conditions and vice versa is defined by a critical Reynolds number (Re_C) converted to a critical head difference Δh_{crit} [Shoemaker et al., 2008a]

$$\Delta h_{crit} = \frac{\mathrm{Re}_C\, \nu \Delta L}{K_{lam} d} \tag{16}$$

where ΔL represents the length over which the head difference is measured [L] and K_{lam} is the laminar hydraulic conductivity of the continuum [L/T].

The approach implemented in CFPM2 for calculating horizontal turbulent hydraulic conductivities is based on an approach for simulating turbulent flow in the vicinity of a wellbore [Halford, 2000]. A dimensionless adjustment factor F_{adj} is used to adjust the laminar hydraulic conductivity [Shoemaker et al., 2008a]

$$K_{turb} = F_{adj} K_{lam} \tag{17}$$

where K_{turb} [L/T] represents the turbulent hydraulic conductivity of the continuum. The adjustment factor is

$$F_{adj} = \sqrt{\frac{\mathrm{Re}_C}{\mathrm{Re}}} = \sqrt{\frac{K_{lam}\Delta h_{crit}}{K_{turb}\Delta h}} \tag{18}$$

when $\Delta h > \Delta h_{crit}$ and with $F_{adj} = 1$ when $\Delta h < \Delta h_{crit}$. K_{turb} is determined iteratively. This approach was found to be well suited for describing turbulent flow observed in permeameter tests at low Reynolds numbers [Kuniansky et al., 2008]. The resulting relationship between hydraulic gradient and discharge, however, is found to be different from that predicted by the Manning or Colebrook-White equations (equations 8 and 6, respectively). While the latter predict a power law with an exponent m = 2.0 (compare Figure 1), steady-state flow simulations with CFPM2 yield a power-law exponent m = 1.5 [Reimann et al., 2011]. Consequently, the calculation of the adjustment factor was modified in CFPM2 such that the power-law exponent can be specified by the user [Reimann et al., 2011]. Briefly described, the discharge calculated by the laminar flow equation (Darcy's law) and that calculated by the turbulent flow equation (power law with an exponent m = 2.0) are equal at an intersection point defined by Re_{C2} (Figure 1). For that reason, the following equation can be derived for the turbulent regime

$$q = \sqrt{\frac{I_{C2}}{I}} K_{lam} I \tag{19}$$

where I is the dimensionless hydraulic gradient and I_{C2} is the dimensionless hydraulic gradient where flow transitions from turbulent to laminar. Therefore, the adjustment factor resulting in CTFc with a flow exponent m = 2.0 is obtained as

$$F_{adj} = \sqrt{\frac{I_{C2}}{I}} \tag{20}$$

when $\Delta h > \Delta h_{crit}$ and with $F_{adj} = 1$ when $\Delta h < \Delta h_{crit}$. Accordingly, the friction coefficient of common turbulent flow equations (k_c for the Colebrook-White equation or n for the Manning equation) is represented by the critical Reynolds number Re_{C2}. Because CTFc is based on the generalized power law with m = 2.0 (e.g., the Manning equation equivalent), the critical Reynolds number Re_{C2} was computed according to the Manning equation. Hence, Re_{C2} is linked with the Manning resistance coefficient n, for which appropriate values are available within the literature (compare Table 1), by the following relationship, which is easily derived from equations (1), (2), (8), and (15)

$$\mathrm{Re}_{C2} = \frac{32 r_{hy}^{4/3}}{n^2 g d} \tag{21}$$

To account for hysteresis when transitioning from laminar to turbulent flow, the critical Reynolds number Re_{C1}, is expressed as a multiple of Re_{C2}

$$\mathrm{Re}_{C1} = \varphi \mathrm{Re}_{C2} \tag{22}$$

where φ represents the multiplier, which ranges from 1 up to approximately 6, compare Kanda and Yanagiya [2008].

The technical implementation of this approach in CFPM2 and its verification using a single-conduit setup are described by Reimann et al. [2011]. In the present work the model is applied to a coupled conduit-matrix flow system and compared to the hybrid model CFPM1.

The impact of the linear head-dependent transfer term to control the conduit inflow capacity, which is used in hybrid models (compare section 3.1), is considered in CTFc by the Horizontal Flow Barrier Package (HFB) for MODFLOW [Hsieh and Freckleton, 1993].

4. Karst Spring Response to Recharge Events in Coupled Conduit-Matrix Systems

Karst systems consist of highly conductive conduits interacting with a matrix (Figure 2). These conduits have a complex configuration and connectivity. Application of the model approaches described herein for a field situation that includes the complexity and uncertainty of a real catchment would be beyond the scope of this study. Hence, a model study in a realistic but relatively simple scenario was performed to (1) compare the SCM approaches (existing CFPM2 [Shoemaker et al., 2008a], modified CFPM2 resulting in CTFc [Reimann et al., 2011], and MODFLOW-2005 [Harbaugh, 2005]) as well as HM approaches (CFPM1 [Shoemaker et al., 2008a]); (2) examine the influence of turbulent flow on karst spring responses; (3) investigate the influence of the matrix properties on karst spring responses; (4) examine the impact of the water transfer coefficient that controls the interaction of conduit and matrix, and (5) investigate the influence of matrix spatial discretization on karst spring responses.

4.1. Study Setup

A single conduit with a length of 1,200 m is coupled to a matrix system to examine the matrix-conduit hydraulic interaction on short-term karst-spring responses after recharge events [Birk et al., 2006]. The width of both columns Δx and rows Δy is set to 50 m except for cells adjacent to the karst conduit centered in the synthetic catchment, where the width of the rows decreases successively to 0.2 m (50, 35, 20, 10, 5.5, 2.5, 1.5, 0.4, 0.2 m respectively). The matrix is represented as a confined / unconfined layer with a thickness of 1,000 m. The diameter d of the karst conduit is 0.2 m with a pipe roughness k_c of 0.01 m, which is approximately equal to a Manning's n of 0.0183 s/m$^{(1/3)}$ and therefore adequate for a small natural flow structure (compare equation 10 and Table 1). For the continuum models, the karst conduit is represented by highly conductive cells with $\Delta y = 0.200$ m and a thickness $\Delta z = 0.157$ m, i.e. the flow cross-section is equal to that of the pipe. The equivalent laminar hydraulic conductivity $K_{lam,c}$ of these cells can be determined using equation 15 yielding 9,374.8 m/s. The critical Reynolds number Re_{C2}, which defines turbulent flow, can be computed by using equation 21 yielding 892.9. The model setup is illustrated in Figure 4.

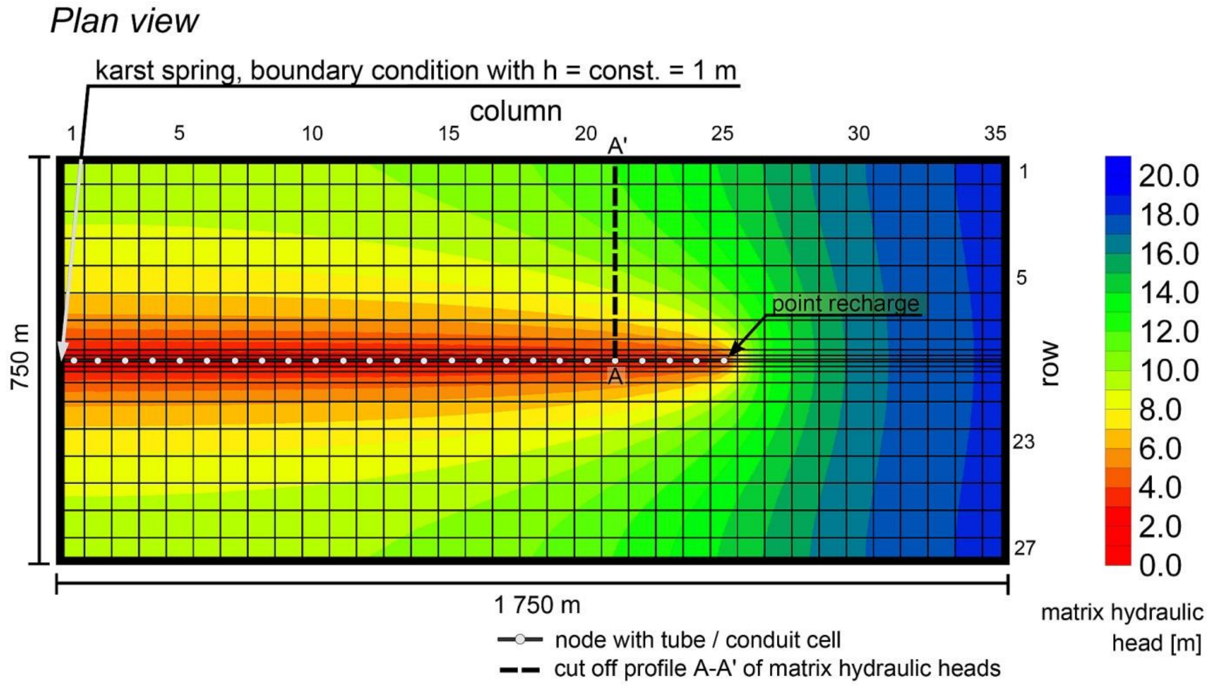

Figure 4: Model domain with steady-state hydraulic heads with a single conduit coupled to the matrix (computed by CTFc with $K_{m1} = 1 \times 10^{-5}$ m/s and $S_m = 0.01$). Grey colored arrow indicates a fixed head boundary while other boundaries are no-flow boundaries.

The discharge area is represented by a fixed hydraulic head of 1 m at the left hand side of the conduit, i.e. flow is from right to left. The other boundaries of the model domain are Neumann boundaries (no-flow). The entire catchment is supplied with constant diffuse recharge of 6.39 x 10^{-9} m/s. Starting at t = 0 with the steady-state flow field, a direct recharge pulse is injected at the right hand end of the conduit with a rate of 0.02 m^3/s over a period of t_{event} = 7,200 seconds. Recharge to the matrix remains unchanged. For an isolated conduit (i.e. not coupled to the matrix), the event recharge $Q_{event}(t)$ is immediately passed through resulting in a spring response $Q_{noexch}(t) = Q_{event}(t) + Q_{base}(t)$ where $Q_{base}(t)$ denotes the spring discharge under steady-state flow conditions without direct recharge. The calculated spring discharge $Q_{model}(t)$ was normalized relative to the pre-recharge event base-flow as $Q_{norm}(t) = Q_{model}(t) / Q_{base}(t)$.

4.2. Benchmark Comparison of Model Approaches

The outlined scenario was used to compare different modeling approaches for a coupled conduit-matrix system. The following numerical models are applied:

(1) MODFLOW-2005 (SCM, laminar flow in the continuum calculated by Darcy's equation).

(2) CFPM1 (HM, laminar flow in the continuum calculated by Darcy's equation, laminar / turbulent flow in a discrete pipe network is simulated by the Hagen-Poiseuille and the Colebrook-White equation). As mentioned above, this approach has been shown to correctly reflect the dual-flow behavior of karst aquifers [Birk et al., 2005; Hill et al., 2010]. Hence, this model approach provides a reference to which other simulations are compared.

(3) CFPM2 (SCM, laminar flow determined using Darcy's equation, while turbulent flow in the continuum is estimated by adjusting the hydraulic conductivity as described by Shoemaker et al. [2008a]).

(4) Modified CFPM2 to result in CTFc (SCM, laminar flow calculated by Darcy's equation, while turbulent flow in the continuum is provided by a power law with an exponent of m = 2.0 [Reimann et al., 2011]).

The matrix conductivity and matrix storage were set to $K_{m1} = 1 \times 10^{-5}$ m/s and $S_m = 0.01$. The f_{ex} threshold value, which creates additional flow resistance between matrix and conduit, was approximated as 12.5. The inverse distance (α in equation 13) used to compute the f_{ex} threshold value was assumed as 0.05 m, which is one fourth of the cell-width where nodes are coupled to the continuum. Accordingly, the exchange factor f_{ex} of the hybrid model was set to a very large value of 125, which is approximately ten times the threshold value, to minimize conduit-matrix flow resistance, because there is no equivalent parameter in the SCM approach.

Figure 5 shows a very close match of the results computed with the CTFc with m = 2.0 and the CFPM1 hybrid model based on the Colebrook-White equation. Hence, CTFc reproduces the dynamic response of a karst spring as well as the hybrid model. In contrast, both MODFLOW-2005 and the existing CFPM2 yield less damped spring responses, i.e. the spring discharge is overestimated relative to the discharge computed by the HM CFPM1. If only laminar flow is considered (MODFLOW-2005) or if turbulent flow is represented by gradient-discharge relationship that obeys a power law with an exponent m = 1.5 (CFPM2), the continuum model fails to reproduce the dynamic response of the spring as predicted by a hybrid model that provides a straightforward representation of the coupled conduit-matrix flow system. This statement is not affected by the slight oscillation in the CFPM2 that results immediately after the increase in spring discharge.

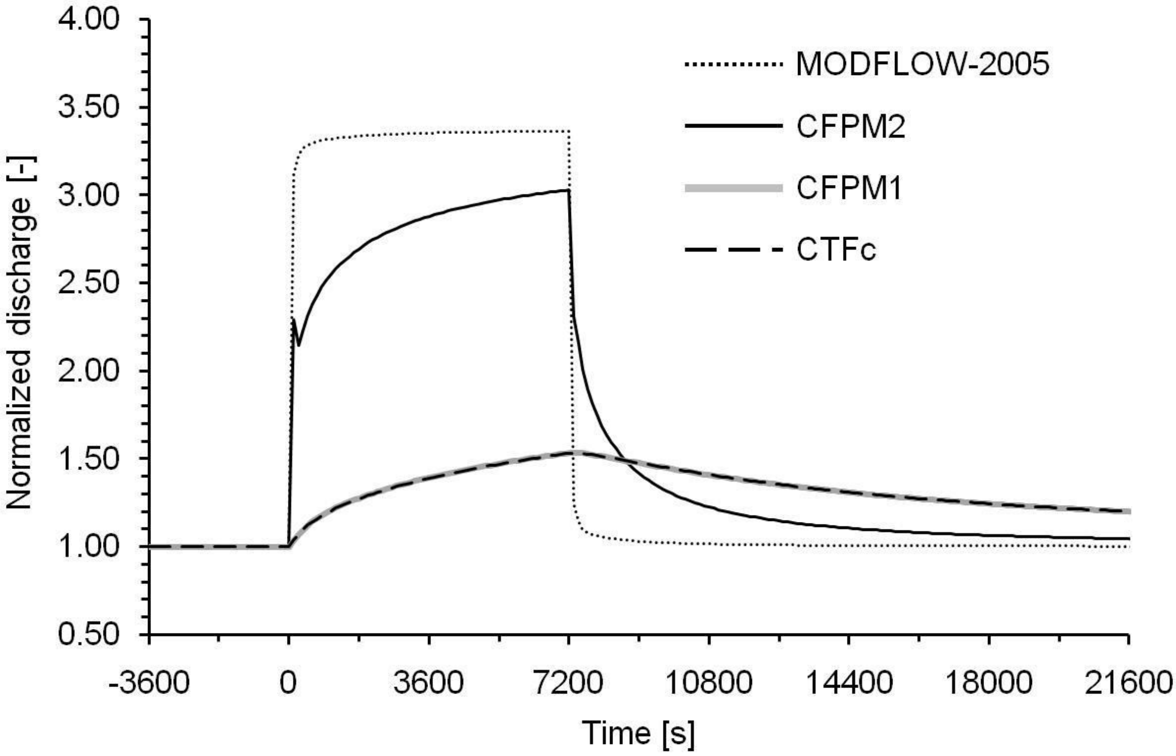

Figure 5: Model comparison for the synthetic catchment.

Successful performance of the CTFc approach is premised on (1) continuum cells that were discretized to represent the area of the karst conduit; and (2) an adequate critical Reynolds number Re_{C2} for the transition from turbulent to laminar flow conditions, which is consistent with the intended flow resistance (e.g. according to Manning's equation). Whether an adequate discretization (premise 1) can be achieved in practical applications and how far this affects the performance of the turbulent continuum model need to be further examined by site-related model applications. Identification of an adequate value of Re_{C2} (premise 2), in principle, requires knowledge about the geometric and hydraulic properties of the karst conduits (compare equation 20). Re_{C2} also may be determined by model calibration in practical applications where information about conduit properties is lacking.

4.3. Parameter Study

The parameter study aims to investigate the influence of the matrix hydraulic properties (section 4.3.1), the conduit-matrix interaction (sections 4.3.2 and 4.3.4), as well as the influence of the matrix spatial discretization on karst spring responses (section 4.3.3). To quantify the effect induced by parameter variation on spring discharge, the spring response of the isolated conduit Q_{noexch} and that of the conduit-matrix system Q_{exch} are compared using the ratio of the respective water volumes discharged at the spring within the event duration t_{event} = 7.200 seconds

$$\lambda_Q = \frac{\int_{t=0}^{t_{event}} \left[Q_{exch}(t) - Q_{base}(t)\right] dt}{\int_{t=0}^{t_{event}} \left[Q_{noexch}(t) - Q_{base}(t)\right] dt} \tag{23}$$

where λ_Q is termed the signal transmission factor [-]. A smaller signal transmission factor indicates less water is discharged to the spring due to interaction with the matrix.

Consequently, $\lambda_Q = 1.0$ means that the matrix does not affect the discharged water volume within the event duration.

4.3.1. Influence of Matrix Parameters for Water Transfer between Matrix and Conduit

To investigate the influence of matrix hydraulic properties on spring discharge, matrix hydraulic parameters are considered by 100 different realizations of randomly generated K_{m1} and S_m values with K_{m1} ranging from 1 x 10^{-8} to 1 x 10^{-4} m/s and S_m ranging from 0.005 to 0.05 [-]. Matrix hydraulic conductivities are assessed according to Kiraly [2002] assuming a controlling length scale for the continuum of approximately 100 m. As before, the exchange factor f_{ex} of the hybrid model was set to a value of 125 to allow unhampered water transfer and, therefore, to allow comparability of model results. Simulated spring flow responses obtained using the SCM approaches CTFc and MODFLOW-2005 as well as the HM approach CFPM1 were compared.

CTFc reproduces normalized discharge simulated by the hybrid model CFPM1 reasonably well (Figure 6a-c). The magnitude and timing of both the rise and recession in normalized discharge are similar for both CTFc and the hybrid model CFPM1. Comparable performance between CTFc and CFPM1 was robust over the range in parameter realizations for K_{m1} and S_m. The laminar flow model MODFLOW-2005 overestimates peak normalized discharge by about 100% due to the lack of turbulent flow.

The signal transmission factor λ_Q (equation 23) was analyzed with respect to hydraulic properties of the matrix. For the scenarios presented here, spring response was insensitive to matrix storage. However, spring responses simulated with CTFc and CFPM1 were sensitive to the hydraulic conductivity of the matrix. Similar to the normalized discharge comparison, the sensitivity of the signal transmission factor λ_Q to matrix hydraulic conductivity computed by CTFc and CFPM1 agree reasonably well (Figure 6a-b, d-e) over the range in parameter realizations for K_{m1} and S_m. The lower the matrix conductivity the less the influence of matrix flow on conduit flow, which is indicated by an increasing signal transmission factor λ_Q (compare Figure 6 d-f). The laminar MODFLOW-2005 greatly underestimates the sensitivity of λ_Q to K_{m1} due to reduced exchange flow between conduit and matrix.

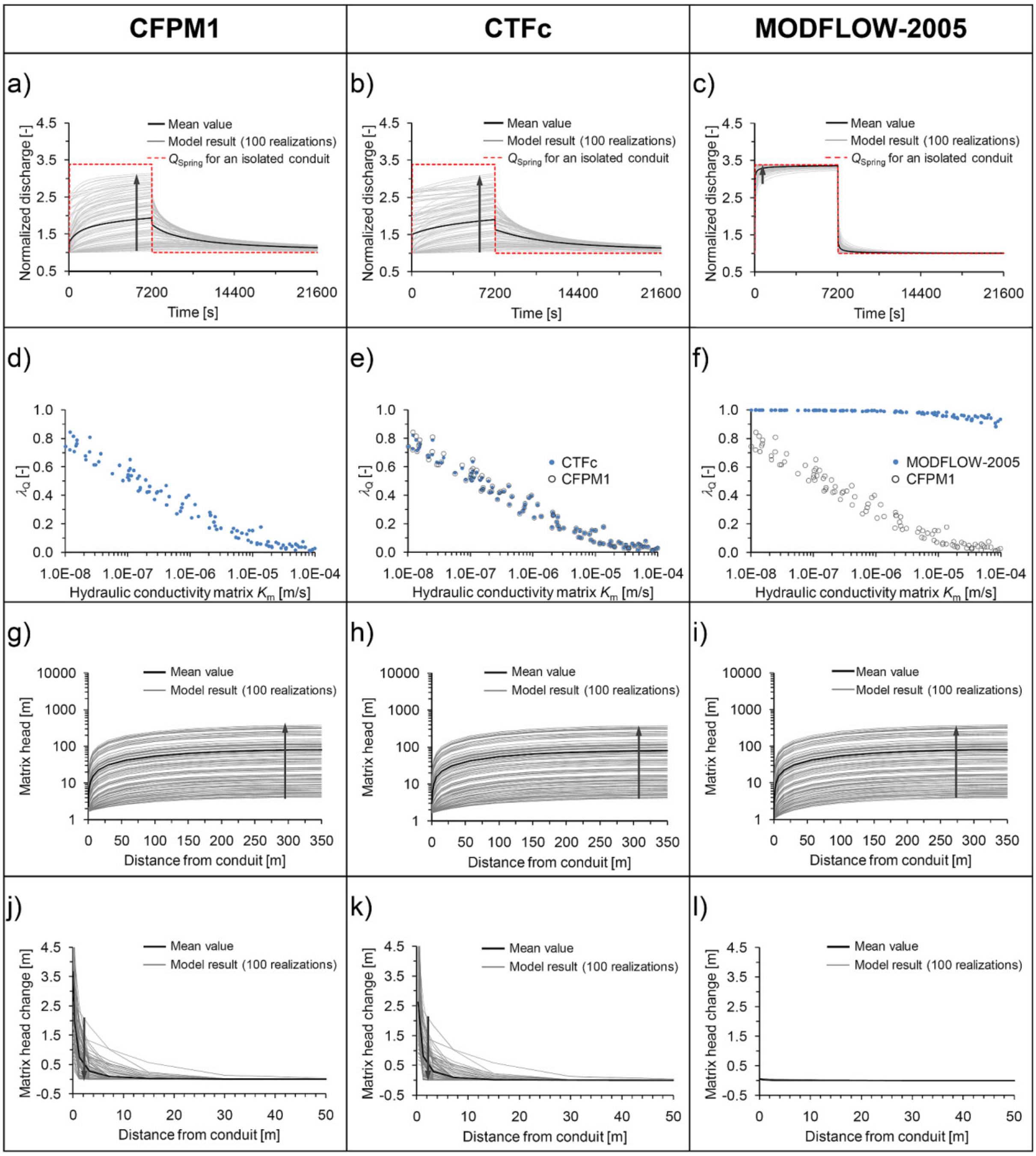

Figure 6: Variation of matrix hydraulic parameters; the grey arrows indicate the direction of decreasing K_{m1} / S_m values; (a) – (c) Spring discharge normalized with respect to the pre-event base-flow, normalized spring discharge computed as $Q_{norm}(t) = Q_{model}(t)/Q_{base}(t)$, (d) – (f) signal transmission factor (ratio between water volumes discharged by conduit-matrix system and isolated conduit within recharge period) and comparison of hybrid model results (CFPM1) to the continuum models CTFc (e) and MODFLOW-2005 (f), (g) – (i) steady-state matrix heads along the cross-section A-A' (compare Figure 4), and (j) – (l) matrix head

change at the end of the recharge period at t = 7,200 s. Results were computed using CFPM1, CTFc, and MODFLOW-2005, respectively.

Matrix hydraulic heads perpendicular to the conduit along the cross-section A-A' (Figure 4) were examined for laminar and turbulent spring flow simulations (Figure 6 g-i). Under steady-state conditions, flow in the conduit is turbulent with Re at the spring ~ 40,000. Due to turbulence, the conduit head is elevated for CTFc and CFPM1 as compared to MODFLOW-2005 as indicated by the associated matrix head near the conduit. Besides this, steady-state matrix heads are comparable for all models (Figure 6g-i). The pulse recharge in turbulent flow conduits increased Re at the spring to ~ 41,700 to 127,000 (depending on the matrix parameters) and causes comparably steeper hydraulic gradients (see also Figure 1) resulting in increased flow from the conduit to the matrix. Hydraulic heads in the surrounding matrix reflect this behavior, whereas the response of matrix hydraulic heads in the laminar model is less pronounced than in the turbulent models (Figure 6j-l).

4.3.2. Limiting Exchange Flow

Commonly, HMs couple matrix and conduit using a linear water exchange factor (equation 13). A priori, this exchange factor is not considered by SCMs. Volumetric exchange between conduit cells and the matrix, however, can be limited by the Horizontal Flow Barrier (HFB) Package [Hsieh and Freckleton, 1993]. This could be important as previous investigations by Peterson and Wicks [2005] suggest that only a limited portion of water is transferred from the conduit to the matrix. Hence, the influence of hybrid model exchange factors f_{ex} on spring flows and matrix heads is further examined using CFPM1, CTFc and MODFLOW-2005. Experimental simulations were performed to determine if hybrid model exchange factors can be duplicated with SCM's using the HFB Package. To this end, the exchange factor f_{ex} was systematically varied for CFPM1 experimental simulations. Based on the basic model setup with K_{m1} = 1 x 10^{-5} m/s and S_m = 0.01, f_{ex} ranged from 100 to 0.001 in 100 equal steps. For the SCMs CTFc and MODFLOW-2005, the exchange factor was transformed into equivalent hydraulic characteristics of the HFB package. Comparison of the equation implemented in the HFB package (compare Hsieh and Freckleton [1993]) and equation 13, which is employed by CFPM1, reveals that the barrier hydraulic conductivity divided by the width of the barrier between two cells, HYDCHR, can be computed as

$$HYDCHR = \frac{f_{ex} K_{m1}}{h_{sat}} \tag{24}$$

where h_{sat} is the average saturated thickness of the conduit cell and the adjacent cell, which is computed by CFPM1. The result from this calculation has to be divided by two as flow barriers were positioned on both sides of conduit-representing cells, whereas in CFPM1 the exchange occurs only within the cells coupled to conduits.

Normalized spring discharge for CFPM1 and CTFc with HFB show a very close match over the range of parameter realizations for the exchange factor f_{ex}. Normalized discharge for the laminar MODFLOW-2005 with HFB clearly differs from turbulent approaches. The recharge pulse is more or less unaffected as the pulse is routed through the conduit (Figure 7a-c). The signal transmission factor illustrates the damping behavior related to exchange factors for turbulent flow models (Figure 7d-f). If the exchange factor is larger than a threshold value, strong damping of spring discharges occurs. The damping gradually diminishes with decreasing exchange factor. If the exchange factor is low, the conduit and the matrix are only weakly coupled and exchange flow between conduit and matrix is low. Therefore, the recharge pulse is directly transmitted to the spring (Figure 7a-f) and results for laminar and turbulent models are similar, at least for the setting considered here.

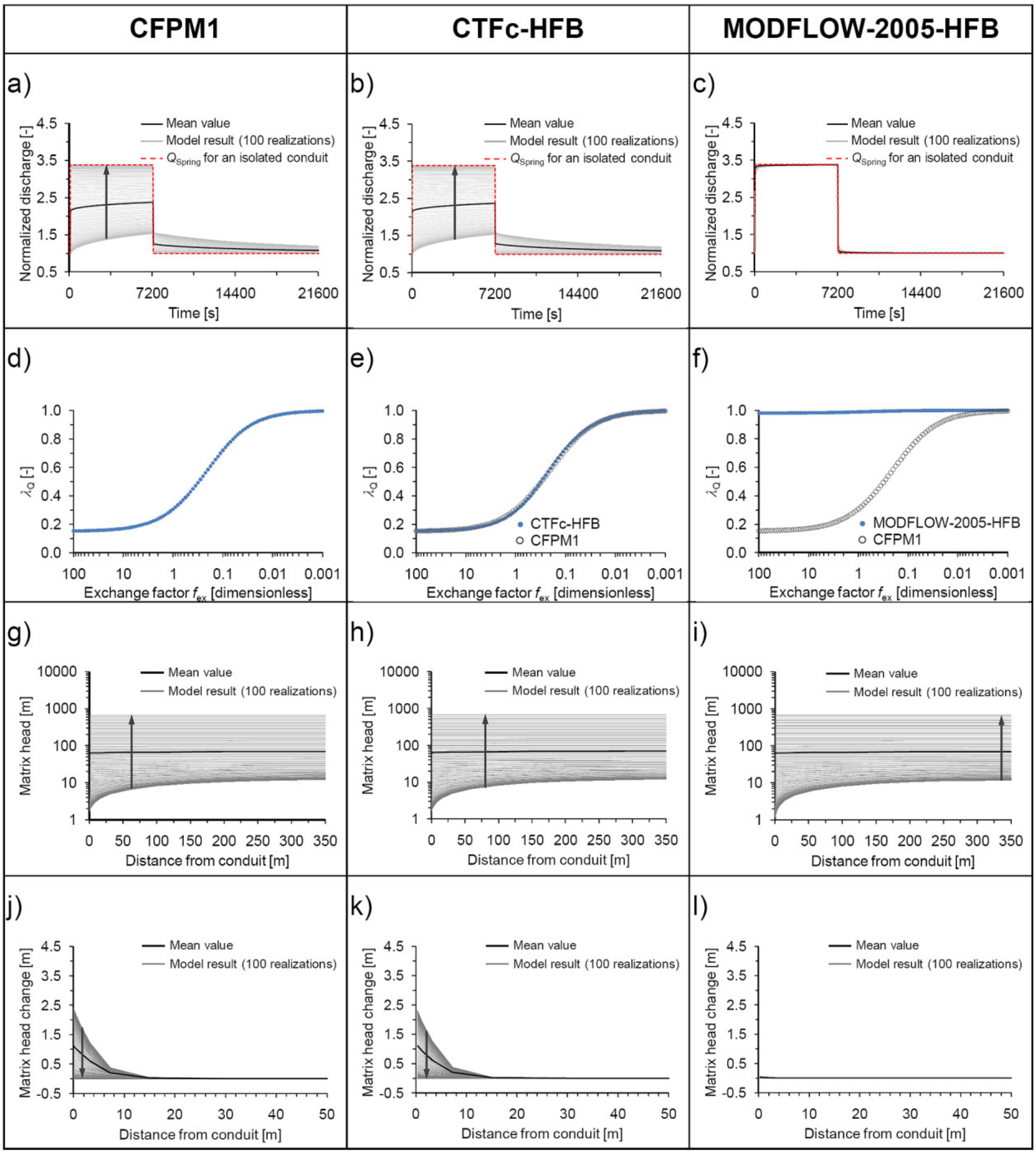

Figure 7: Variation of the exchange factor f_{ex}; the grey arrows indicate the direction of decreasing f_{ex}; (a) – (c) Spring discharge normalized with respect to the pre-event base-flow, normalized spring discharge computed as $Q_{norm}(t) = Q_{model}(t)/Q_{base}(t)$. (d) – (f) signal transmission factor (ratio between water volumes discharged by conduit-matrix system and isolated conduit within recharge period) and comparison of hybrid model results (CFPM1) to the continuum models CTFc (e) and MODFLOW-2005 (f),, (g) – (i) steady-state matrix heads along the cross-section A-A' (compare Figure 4), and (j) – (l) matrix head change at the end

of the recharge period at t = 7,200 s. Results were computed using CTFc, CFPM1, and MODFLOW-2005, respectively.

Steady-state matrix heads along the cross section A-A' illustrate the meaning of the exchange factor (Figure 7g-i). Large exchange factors allow extensive drainage resulting in comparatively low matrix heads. With this, the conduit acts similar to an internal fixed head boundary condition. If the exchange factor falls below the threshold, the additional resistance alters the conduit behavior from a fixed head to a flux-dependent head (Cauchy) condition. The smaller the exchange factor the higher the matrix heads. This behavior is similar for laminar and turbulent models. However, both laminar and turbulent approaches differ with respect to the matrix head change induced by the recharge pulse (Figure 7j-l). For laminar flow models, matrix heads around the conduit seem to be unaffected by the recharge pulse whether exchange factors are high or low. In contrast, the matrix head changes near the conduit are considerable for turbulent models (CFPM1 and CTFc-HFB), especially when exchange factors f_{ex} are large (Figure 7j-l).

4.3.3. Sensitivity of Exchange Flow to Matrix Spatial Discretization

Next, the influence of the matrix spatial discretization was briefly investigated, as this potentially affects the interaction between turbulent flow conduits and matrix cells. The matrix spatial discretization of rows Δy was increased for CFPM1 and CTFc up to around 50 m whereas the conduit-representing cell in CTFc remains at Δy = 0.2 m in order to allow comparable flow computation. The HFB flow barrier characteristic was parameterized equal to the model run with close-meshed matrix discretization. Additionally, for one CFPM1 model scenario, the continuum-cell interacting with the conduit-cell was set to Δy = 0.2 m as used for the scenario with close-meshed matrix discretization. As in the previous model runs, the exchange factor f_{ex} was varied from 100 to 0.001 in 100 equal steps.

Normalized discharge for model runs with larger cells clearly differs from the previously investigated standard scenario (Figure 8a-f). If the conduit interacts with large continuum cells (left hand side of Figure 8), water may enter a large aquifer volume without appropriate resistance behavior resulting in some artificial damping (Figure 8a). The signal transmission factor supports this finding as the values are very low for large exchange factors (Figure 8d). With a decreasing exchange factor, water flow between the conduit and the matrix is reduced and, therefore, the significance of matrix discretization is diminished. If the discrete conduit interacts with comparably small continuum cells (middle column of Figure 8), water transfer is not artificially damped by a large and slow reacting continuum cell. However, due to head-averaging in the large surrounding cells, the hydraulic gradient from the conduit to the matrix is artificially somewhat reduced resulting in slightly enhanced water flow perpendicular to the conduit that results in slightly more damping of conduit flow (compare Figures 8b,e,h,k and 7a,d,g,j). CTFc-HFB shows a similar behavior as CFPM1 with small interacting cells because turbulent conduit flow interacts with the matrix continuum in a similar manner.

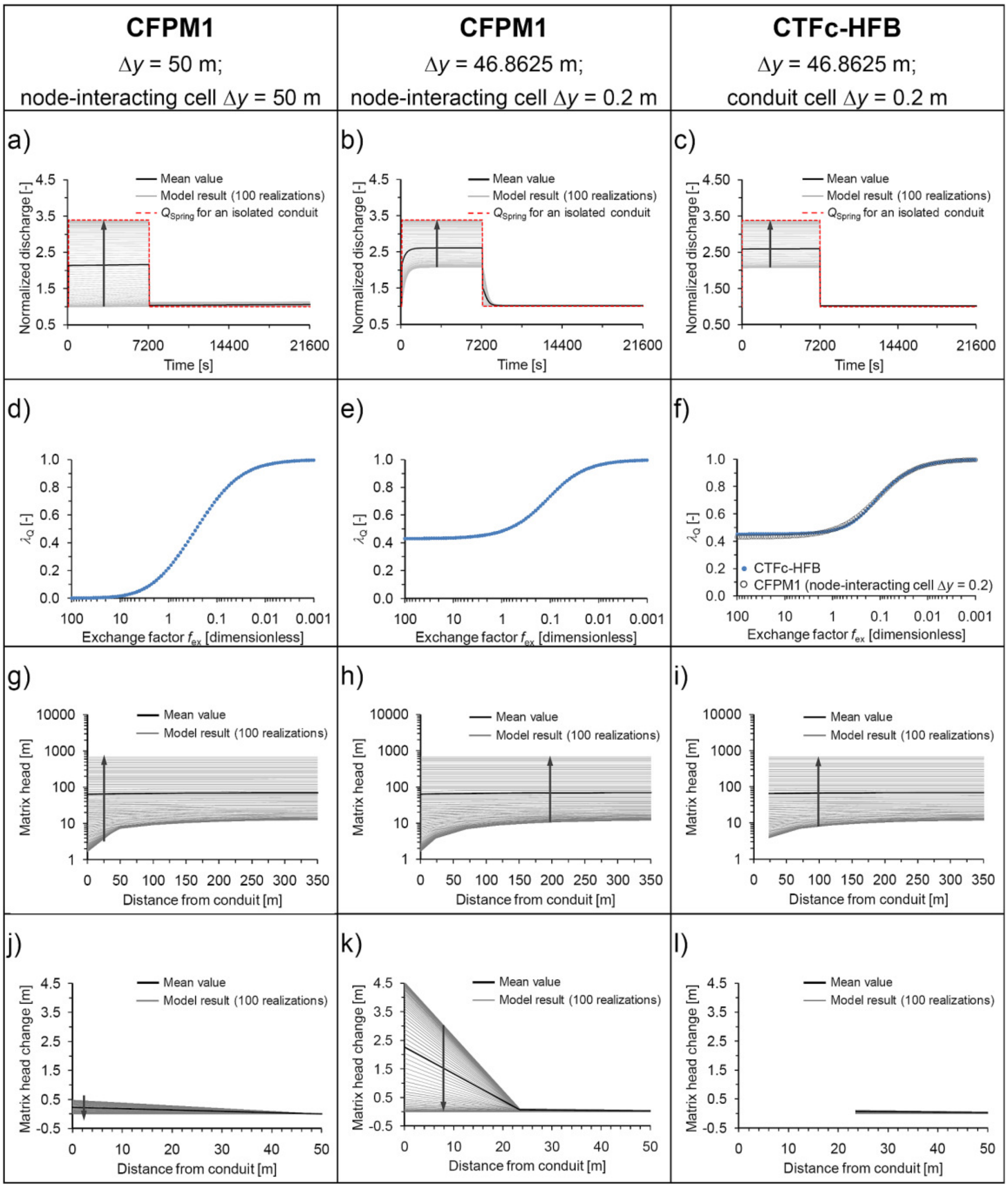

Figure 8: Influence of spatial discretization of the continuum model; the grey arrows indicate the direction of decreasing f_{ex}; (a) – (c) Mean normalized discharge; (d) – (f) signal transmission factor (ratio between water volumes discharged by conduit-matrix system and isolated conduit within recharge period) as well as the difference between hydraulic heads in the matrix and the conduit. (g) – (i) matrix heads perpendicular to the conduit for steady-state conditions prior to the recharge pulse; (j) – (l) matrix head variation due to the recharge pulse. Results were computed using CTFc with HFB and CFPM1.

4.3.4. Influence of Matrix Parameters on Spring Flow in Dependency of the Exchange Factor

Next, the influence of the exchange factor for several model settings with varying matrix parameter settings was investigated. To this end, the exchange factor was varied for three CFPM1 model runs as 12.5, 0.125, and 0.025, representing three different scalings of the hydraulic conductivity, as mentioned above (section 3.1). Each model run consists of 100 random realizations for matrix hydraulic conductivity K_{m1} and storage S_m as described in section 4.3.1.

Normalized discharge generally increases as the exchange factor f_{ex} decreases (Figure 9a-c). As expected, decreasing the exchange factor f_{ex} gradually decouples the conduit and matrix flow interaction. As the exchange factor f_{ex} approaches zero, normalized discharge for the CFPM1 hybrid model resembles normalized discharge simulated by the laminar flow model MODFLOW-2005 (Figure 9a-c and Figure 6a-c).

A decreasing exchange factor f_{ex} changes the sensitivity relation between λ_Q and K_{m1} (Figure 9d-f). The relatively large exchange factor f_{ex} equal to 12.5 increases the exchange flow and therefore the sensitivity of λ_Q to K_{m1}. More specifically, λ_Q is relatively sensitive to the entire range of K_{m1} tested in this study when the exchange factor f_{ex} equals 12.5 (Figure 9d). The signal transmission factor λ_Q is relatively insensitive to K_{m1} less than about 1.0 x 10^{-6} m/s, when the exchange factor f_{ex} equals 0.125 (Figure 9e). Likewise, λ_Q is relatively insensitive to K_{m1} less than about 1.0 x 10^{-5} m/s, when the exchange factor f_{ex} equals 0.025 (Figure 9f). This behavior is consistent as smaller exchange factors result in diminished exchange flow. This effect is increased by decreasing matrix conductivity K_{m1} (compare equation 13) because the exchange factor in this study depends on this parameter.

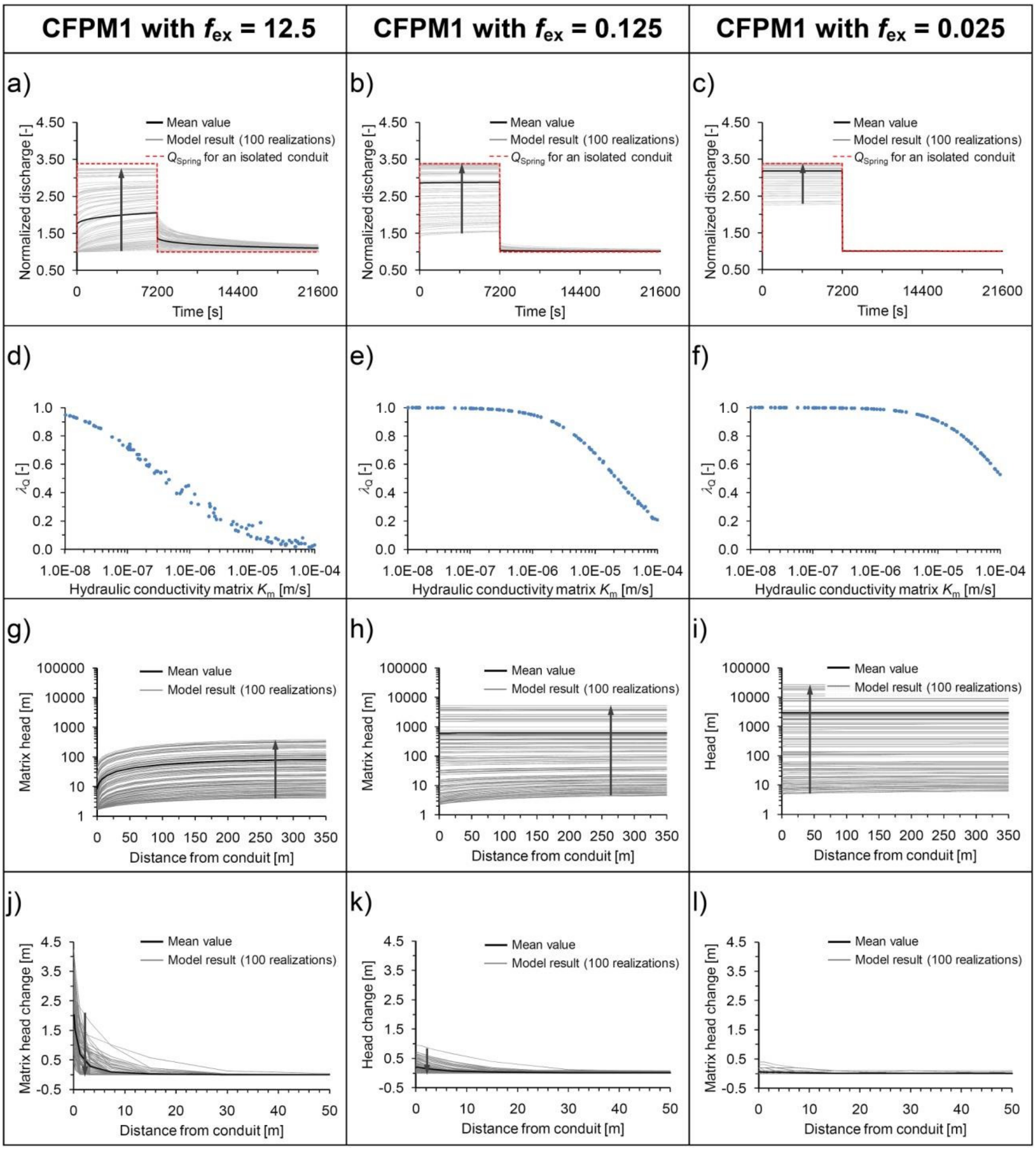

Figure 9: Influence of exchange factor f_{ex} on model results for a wide variety of matrix parameters computed with CFPM1; the grey arrows indicate the direction of decreasing K_{m1} / S_m values; (a) – (c) Mean normalized discharge; (d) – (f) signal transmission factor (ratio between water volumes discharged by conduit-matrix system and isolated conduit within recharge period) as well as the difference between hydraulic heads in the matrix and the conduit. (g) – (i) matrix heads perpendicular to the conduit for steady-state conditions prior to the recharge pulse; (j) – (l) matrix head variation due to the recharge pulse.

Matrix heads clearly vary over the whole range of matrix hydraulic parameters (Figure 9g-i) with a variability exceeding several orders of magnitude. This effect is emphasized by decreasing the exchange factor. Use of a small exchange factor together with low hydraulic conductivity results in implausible matrix heads indicating that the reasonable range of parameters is exceeded (Figure 9g-i).

The influence of turbulent conduit flow on the variability of matrix hydraulic heads due to the variability of conduit flow diminishes if the exchange factor is further reduced in the hybrid model (Figure 9j-l). Again, the smaller the exchange factor the more the conduit and matrix are hydraulically decoupled (Figure 9g-l). Matrix hydraulic heads in the investigated model setting, therefore, depend on the transfer coefficient as well as on the matrix hydraulic parameters (compare Figures 7g-i and 9g-i). In practical model applications, the exchange factor therefore may be found useful for adjusting the model to measured responses of the spring or the hydraulic heads in the matrix. This, however, bears the risk that the exchange factor is utilized to compensate for deficiencies in the conceptual model or errors in other model parameters such as net recharge and matrix hydraulic conductivity.

5. Conclusions

A new approach (CTFc) to simulate laminar and turbulent flow using a single-continuum model is tested for consistency with a more complex and physics-based hybrid model approach. CTFc simulates turbulent flow using a power law with a flow exponent $m = 2.0$. Analyses of the underlying laminar and turbulent flow equations allowed adequate CTFc parameterization for testing purposes. With this, dual-porosity flow components of karstic aquifers can be simulated within a single continuum where karst conduits are represented by highly-conductive model cells. CTFc successfully simulates spring discharge of a conduit system embedded within a porous-medium matrix.

CTFc results agree well with those computed by the hybrid model CFPM1, which explicitly accounts for turbulent conduit flow using a discrete pipe network. A comparison of turbulent single-continuum and hybrid flow models with the traditional laminar MODFLOW-2005 reveals the impact of turbulent flow on spring flow induced by recharge events particularly for comparably high conductive matrix settings with effective conduit-matrix interaction. Spring-flow dynamics are found to be strongly influenced by conduit hydraulics. Accordingly, the shape of the spring hydrograph predicted by a model that accounts for turbulent flow conditions differs from that obtained with a laminar model approach. For karst systems with a highly conductive matrix, a conventional laminar MODFLOW-2005 model greatly overestimates peak spring discharge and underestimates hydraulic gradients within the conduit. This results in reduced conduit flow interaction with the matrix. Spring flow responses to recharge events are poorly damped when compared with simulated estimates that account for transitional and turbulent flow.

Hybrid models couple discrete pipe-like conduits to a continuum domain and use an exchange factor to control the transfer of groundwater between the matrix and the conduit system. For sufficiently high exchange factors, simulation results obtained with CTFc are found to be as adequate as those simulated with the hybrid model CFPM1. By reducing the value of the exchange factor, however, hybrid models are able to consider limited hydraulic interaction between karst conduits and the matrix, which may correspond to a reduced conduit infiltration capacity, e.g., due to the scale dependency of hydraulic properties. CTFc mimics the limited hydraulic interaction by use of the HFB package for MODFLOW, which is proven here by 2D parameter studies. Therefore, the numerically simpler CTFc approach is believed to offer a reasonable alternative to the more demanding hybrid models in practical applications addressing karst aquifers.

More generally, this study suggests that inferences of aquifer properties from spring hydrographs are potentially impaired by ignoring turbulent flow effects. Therefore, adequate representation of turbulent flow conditions in karst models may deserve equal or greater attention than focusing on the general pros and cons of continuum and hybrid models discussed in the literature. It is admitted that discharge hydrographs simulated in this paper were highly simplified. Hence, future work will have to substantiate the conclusions drawn herein using more complex models of real karst catchments.

Acknowledgements

This work was funded by the Deutsche Forschungsgemeinschaft (DFG, German Research Foundation) under grants no. LI 727/11-1 and SA 501/24-1 and the Austrian Science Fund (FWF) under grant no. L576-N21. The authors express their appreciation to Robert A. Renken, Andrew J. Long, and Eric D. Swain of the USGS and Rudolf Liedl from the TU Dresden for their internal review prior to submission to the journal as well as Stephen R. H. Worthington and two anonymous reviewers for their insightful comments that greatly helped to improve the manuscript.

Sadly, we have to report that our colleague and friend Dr. Christoph Rehrl died on 21 March 2010 at the age of 37. His dedication and person were an inspiration to us all.

Reference List

Barenblatt, G. I., I. P. Zheltov, and I. N. Kochina (1960), Basic concepts in the theory of seepage of homogeneous liquids in fissured rock, Journal of Applied Mathematics and Mechanics (PMM), 24(5), 1286–1303.

Bauer, S., R. Liedl, and M. Sauter (2003), Modeling of karst aquifer genesis: Influence of exchange flow, Water Resour. Res., 39(10), 1285, doi: 10.1029/2003WR002218.

Bear, J. (1988), Dynamics of fluids in porous media. Repr. Dover (Dover books on physics and chemistry), New York.

Birk, S., T. Geyer, R. Liedl, and M. Sauter (2005), Process-based interpretation of tracer tests in carbonate aquifers, Ground Water, 43(3), 381–388.

Birk, S., R. Liedl, and M. Sauter (2006), Karst spring responses examined by process-based modeling, Ground Water, 44(6), 832–836.

Covington, M. D., C. M. Wicks, and Saar M. O. (2009), A dimensionless number describing the effects of recharge and geometry on discharge from simple karstic aquifers, Water Resour. Res., 45, W11410, doi:10.1029/2009WR008004.

Eisenlohr, L., L. Király, M. Bouzelboudjen, and Y. Rossier (1997), Numerical simulation as a tool for checking the interpretation of karst spring hydrographs, Journal of Hydrology, 193, 306–315.

Forchheimer, P. (1901), Wasserbewegung durch Boden, Zeitschr. d. V. deutsch. Ing., 45, 1782–1788.

Ford, D. and P. Williams (2007), Karst Hydrogeology and Geomorphology, John Wiley & Sons Ltd, Chichester, England.

Halford, K. J. (2000), Simulation and interpretation of borehole flowmeter results under laminar and turbulent flow conditions, in Seventh International Symposium on Logging for Minerals and Geotechnical Applications, 157–168. Golden, Colorado.

Harbaugh, A. W. (2005), MODFLOW-2005. The U.S. Geological Survey Modular Ground-Water Model - the Ground-Water Flow Process, U.S. Geological Survey Techniques and Methods 6-A, Reston, Virginia.

Hill, M. E., M. T. Steward, and A. Martin (2010), Evaluation of the MODFLOW-2005 Conduit Flow Process, Ground Water, 48(4), 549-559, doi: 10.1111/j.1745-6584.2009.00673.x.

Hsieh, P. A. and J. R. Freckleton (1993), Documentation of a computer program to simulate horizontal-flow barriers using the U.S. Geological Survey modular three-dimensional finite-difference ground-water flow model, U.S. Geological Survey Open-File Report 92-477, 32 p.

Jain, S. C. (2001), Open-channel flow, John Wiley & Sons, New York.

Kanda, H. and T. Yanagiya (2008), Hysteresis curve in reproduction of Reynolds' color-band experiments, J. Fluid. Eng., 130(5), 051202, doi: 10.1115/1.2903741.

Kaufmann, G. (2009), Modelling karst geomorphology on different time scales, Geomorphology, 106, 62-77, doi: 10.1016/j.geomorph.2008.09.016.

Király, L. (1984), Régularisation de l'Areuse (Jura Suisse) simulée par modèle mathématique, in Hydrogeology of karstic terraines, edited by A. Burger, and L. Dubertret, 94–99, Heise, Hannover.

Király, L. (2002), Karstification and Groundwater Flow. In: Gabrovšek, F. (ed.), Proceedings of the Conference on Evolution of Karst: From Prekarst to Cessation, Postojna-Ljubljana, 155–190.

Kuniansky, E. L., K. J. Halford, and W. B. Shoemaker (2008), Permeameter data verify new turbulence process for MODFLOW, Ground Water, 46(5), 768–771.

Liedl, R., M. Sauter, D. Hückinghaus, T. Clemens, and G. Teutsch (2003), Simulation of the development of karst aquifers using a coupled continuum pipe flow model, Water Resour. Res., 39, 1057, doi: 10.1029/2001WR001206.

Lindgren, R. J., A. R. Dutton, S. D. Hovorka, S. R. H. Worthington, and S. Painter (2004), Conceptualization and simulation of the Edwards Aquifer, San Antonio Region, Texas, Scientific Investigations Report, Reston, Virginia.

Meyer, B. A., Kincaid, T. R., and T. H. Hazlett (2008), Modeling karstic controls on watershed-scale groundwater flow in the Floridian Aquifer of North Florida, in: Yuhr, L. B., E. C. Alexander, Jr., and B. F. Beck (eds), Sinkholes and the engineering and environmental impacts of karst, Geotechnical Special Publication No. 183, American Society of Civil Engineers, Reston, VA, 351-361.

Muskat, M. (1946), The flow of homogeneous fluids through porous media, McGraw-Hill, Ann Arbor, Michigan.

Painter, S. L., A. Sun, and R. T. Green (2006), Enhanced characterization and representation of flow through karst aquifers. Awwa Research Foundation; IWA Publ., London.

Peterson, E. W. and C. M. Wicks (2005), Fluid and Solute Transport from a Conduit to the Matrix in a Carbonate Aquifer System, Mathematical Geology, 37 (8), 851–867.

Peterson, E. W. and C. M. Wicks (2006), Assessing the importance of conduit geometry and physical parameters in karst systems using the storm water management model (SWMM), Journal of Hydrology, 329(1-2), 294–305.

Rehrl, C., S. Birk, and A. B. Klimchouk (2008), Conduit evolution in deep-seated settings: Conceptual and numerical models based on field observations, Water Resour. Res., 44, W11425, doi: 10.1029/2008WR006905.

Reimann, T, S. Birk, C. Rehrl, and W. B. Shoemaker (2011), Modifications to the Conduit Flow Process Mode 2 for MODFLOW-2005, Ground Water, doi: 10.1111/Fj.1745-6584.2011.00805.x.

Scanlon, B. R., R. E. Mace, M. E. Barrett, and B. Smith (2003), Can we simulate regional groundwater flow in a karst system using equivalent porous media models? Case study, Barton Springs Edwards aquifer, USA, Journal of Hydrology, 276(1-4), 137–158.

Şen, Z. (1995), Applied Hydrogeology for scientists and engineers, CRC Press Inc, Boca Raton, Florida.

Shoemaker, W. B., E. L. Kuniansky, S. Birk, S. Bauer, and E. D. Swain (2008a), Documentation of a Conduit Flow Process (CFP) for MODFLOW-2005, U.S. Geological Survey Techniques and Methods Book 6, Chapter A, Reston, Virginia.

Shoemaker, W. B., K. J. Cunningham, E. L. Kuniansky, and J. Dixon (2008b), Effects of turbulence on hydraulic heads and parameter sensitivities in preferential groundwater flow layers, Water Resour. Res., 44, W03501, doi: 10.1029/2007WR006601.

Teutsch, G., and M. Sauter (1998), Distributed parameter modeling approaches in karst-hydrological investigations, Bulletin d'Hydrogéologie, 16, 99–109.

Worthington, S. R. H. (2009), Diagnostic hydrogeologic characteristics of a karst aquifer (Kentucky, USA), Hydrogeology Journal (17), 1665–1678.

Young, D. F., B. R. Munson, and T. H. Okiishi (2004), A brief introduction to fluid mechanics, 3rd ed., Wiley, Hoboken, NJ.

Figure captions

Figure 1: Hydraulic gradient and corresponding discharge for different linear (laminar flow) and nonlinear (turbulent flow) equations. The example is computed for a conduit with d = 0.2 m, k_c = 0.01 m, and n = 1.83 x 10^{-2} s/$m^{(1/3)}$.

Figure 2: Cross section of a karst conduit embedded in the matrix. The flow system is controlled by matrix flow to karst conduits (Q_m), conduit infiltration capacity (Q_i), and conduit flow capacity (Q_c).

Figure 3: Flow rates Q_m/L and Q_i/L for a karst system with a single conduit (d = 0.2 m) for several hydraulic conductivities. With a given amount of water that is gathered by the conduit (Step 1), one can determine the equivalent hydraulic gradient in the matrix towards the conduit. In this example the gradient is approximated by the head difference (assuming h_o = πd/2) perpendicular to the conduit divided by the associated length, which was set equal to 100 m (Step 2a: K_{m1} = 1 x 10^{-5} m/s). The necessary inflow gradient I_{m2} for the conduit can be determined according to the hydraulic conductivity in the matrix in the vicinity of the conduit K_{m2} (Step 2b: K_{m2} = 1 x 10^{-9} m/s). As the inflow gradient I_{m2} clearly exceeds the matrix gradient, matrix heads will clearly exceed conduit heads for this specific parameter set under the assumed conditions.

Figure 4: Model domain with steady-state hydraulic heads with a single conduit coupled to the matrix (computed by CTFc with K_{m1} = 1 x 10^{-5} m/s and S_m = 0.01). Grey colored arrow indicates a fixed head boundary while other boundaries are no-flow boundaries.

Figure 5: Model comparison for the synthetic catchment

Figure 6: Variation of matrix hydraulic parameters; the grey arrow indicate the direction of decreasing K_{m1} / S_m values; (a) – (c) Spring discharge normalized with respect to the pre-event base-flow, normalized spring discharge computed as $Q_{norm}(t) = Q_{model}(t)/Q_{base}(t)$, (d) – (f) signal transmission factor (ratio between water volumes discharged by conduit-matrix system and isolated conduit within recharge period) and comparison of hybrid model results (CFPM1) to the continuum models CTFc (e) and MODFLOW-2005 (f),, (g) – (i) steady-state matrix heads along the cross-section A-A' (compare Figure 4), and (j) – (l) matrix head change at the end of the recharge period at t = 7,200 s. Results were computed using CFPM1, CTFc, and MODFLOW-2005, respectively.

Figure 7: Variation of the exchange factor f_{ex}; the grey arrow indicate the direction of decreasing f_{ex}; (a) – (c) Spring discharge normalized with respect to the pre-event base-flow, normalized spring discharge computed as $Q_{norm}(t) = Q_{model}(t)/Q_{base}(t)$. (d) – (f) signal transmission factor (ratio between water volumes discharged by conduit-matrix system and isolated conduit within recharge period) and comparison of hybrid model results (CFPM1) to the continuum models CTFc (e) and MODFLOW-2005 (f), (g) – (i) steady-state matrix heads along the cross-section A-A' (compare Figure 4), and (j) – (l) matrix head change at the end of the recharge period at t = 7,200 s. Results were computed using CTFc, CFPM1, and MODFLOW-2005, respectively.

Figure 8: Influence of spatial discretization of the continuum model; the grey arrow indicate the direction of decreasing f_{ex}; (a) – (c) Mean normalized discharge; (d) – (f) signal transmission factor (ratio between water volumes discharged by conduit-matrix system and isolated conduit within recharge period) as well as the difference between hydraulic heads in the matrix and the conduit. (g) – (i) matrix heads perpendicular to the conduit for steady-state

conditions prior to the recharge pulse; (j) – (l) matrix head variation due to the recharge pulse. Results were computed using CTFc with HFB and CFPM1.

Figure 9: Influence of exchange factor f_{ex} on model results for a wide variety of matrix parameters computed with CFPM1; the grey arrow indicate the direction of decreasing K_{m1} / S_m values; (a) – (c) Mean normalized discharge; (d) – (f) signal transmission factor (ratio between water volumes discharged by conduit-matrix system and isolated conduit within recharge period) as well as the difference between hydraulic heads in the matrix and the conduit. (g) – (i) matrix heads perpendicular to the conduit for steady-state conditions prior to the recharge pulse; (j) – (l) matrix head variation due to the recharge pulse.

Table captions

Table 1: Values for Manning coefficient n.